Ultrafast magnetization dynamics in Co-based Heusler compounds with tuned chemical ordering

2014 New J. Phys. 16 063068

(http://iopscience.iop.org/1367-2630/16/6/063068)

New Journal of Physics
The open access journal at the forefront of physics
Deutsche Physikalische Gesellschaft DPG | IOP Institute of Physics

Ultrafast magnetization dynamics in Co-based Heusler compounds with tuned chemical ordering

D Steil[1], O Schmitt[1], R Fetzer[1], T Kubota[2], H Naganuma[3], M Oogane[3], Y Ando[3], A K Suszka[4], O Idigoras[4], G Wolf[1], B Hillebrands[1], A Berger[4], M Aeschlimann[1] and M Cinchetti[1]

[1] Department of Physics and Research Center OPTIMAS, University of Kaiserslautern, D-67653 Kaiserslautern, Germany
[2] WPI Advanced Institute for Materials Research, Tohoku University, Sendai 980-8579, Japan
[3] Department of Applied Physics, Graduate School of Engineering, Tohoku University, Sendai 980-8579, Japan
[4] CIC nanoGUNE Consolider, E-20018 Donostia, San Sebastian, Spain
E-mail: cinchett@rhrk.uni-kl.de

Received 23 January 2014, revised 13 May 2014
Accepted for publication 23 May 2014
Published 30 June 2014

New Journal of Physics **16** (2014) 063068
doi:10.1088/1367-2630/16/6/063068

Abstract

We have studied thin film samples of Co_2FeSi and Co_2MnSi with different degrees of chemical ordering using the time-resolved magneto-optical Kerr effect to elucidate the influence of defects in the crystal structure on magnetization dynamics. Surprisingly, we find that the presence of defects does not influence the optically induced magnetization dynamics on the ultrashort timescale (some 100 fs). However, we observe a second demagnetization stage with a timescale of tens of picoseconds in Co_2MnSi for low chemical ordering; that is, a large number of defects. We interpret this second demagnetization step as originating from scattering of mostly thermalized majority electrons into unoccupied minority defect states.

Keywords: ultrafast demagnetization, Heusler compounds, halfmetallic materials, spin dynamics, magnetic properties

1. Introduction

The magnetization dynamics of ferromagnetic materials after excitation with an ultrashort laser pulse has now been a dynamic field of basic research for more than 15 years, starting with the experiments on nickel by Beaurepaire *et al* in 1996 [1]. A wealth of theoretical [2–9] and experimental [10–19] studies on elementary ferromagnets have followed. Today, it is a well established fact that the 3*d*-ferromagnets Co, Fe and Ni show characteristic demagnetization times on the order of a few 100 fs after optical excitation, while 4*f*-magnets exhibit more complicated dynamics with a two-step demagnetization and timescales up to the tens of picosecond range [14, 20]. However, the microscopic mechanism responsible for this dynamics is still debated (for a partial overview see, e.g., [21]).

More recently, complex material systems, like half-metallic ferromagnets [22–28] or ferrimagnetic alloys [29–35] have become a focus of investigation. These systems are not only interesting from a fundamental point of view, but also for technological applications in spin electronics (spintronics) and data storage [36–38]. Half-metallic Heusler compounds, for example, constitute ideal building blocks for all types of spintronics devices. Due to the fact that a band gap exists in one of the spin channels at the Fermi energy (E_F), they can provide fully spin-polarized currents, which is a main basic ingredient for spin electronics. For a detailed overview of the manifold of properties of Heusler systems see [39].

From a more fundamental point of view, it is intriguing to ask how the band gap in one spin channel influences ultrafast magnetization dynamics [22, 23, 25]. It is already known that some half metals like CrO_2 exhibit very slow dynamics on the order of hundreds of picoseconds [22], while the Co-based Heusler compounds with composition Co_2YZ generally show demagnetization dynamics with timescales comparable to the 3*d*-ferromagnets [22–26, 40]. One possible interpretation of this fast dynamics is that the half-metallicity of the Heusler compounds is destroyed by defects in the crystal structure (i.e., a lowered chemical ordering), which leads to a non-vanishing density of states (DOS) within the spin band gap around the Fermi energy [41–44]. The two most prominent examples of such defects are Co atoms displaced at the Y lattice positions (Co_Y antisites) and intermixing of Y atoms with the Z species at their respective lattice positions. While the former kind of disorder is quite robust against annealing procedure [45], the latter can be overcome to a high amount by heat treatment, as observable by x-ray diffraction (XRD) measurements (see e.g. [46]).

Another interpretation that has been given to explain the ultrafast dynamics observed in Heusler compounds is that the band gap, typically around 0.5–1.0 eV in calculations, is too small to prohibit ultrafast dynamics [22, 25]. Some of the present authors have studied the influence of the band gap on the magnetization dynamics for the Heusler compounds Co_2FeSi (CFS) and Co_2MnSi (CMS), both experimentally and using energy- and momentum-resolved calculations of electron dynamics [23]. It was shown that, even for perfect half-metallicity, ultrafast demagnetization in the sub-picosecond timescale is possible. As schematically shown in figure 1, the dynamics in such systems is governed by hole-mediated spin-flip scattering below the Fermi energy, which is indeed possible because the photon energy of the exciting laser is larger than the spectral width of the minority gap. Since the relevant spin-flip dynamics happen below the band gap, the different energetic position of the band gap with respect to E_F in CFS and CMS does not influence the ultrafast demagnetization.

In this article, we extend the time-resolved magneto-optical Kerr effect (TR-MOKE) studies of the Heusler compounds CFS and CMS by considering samples with different

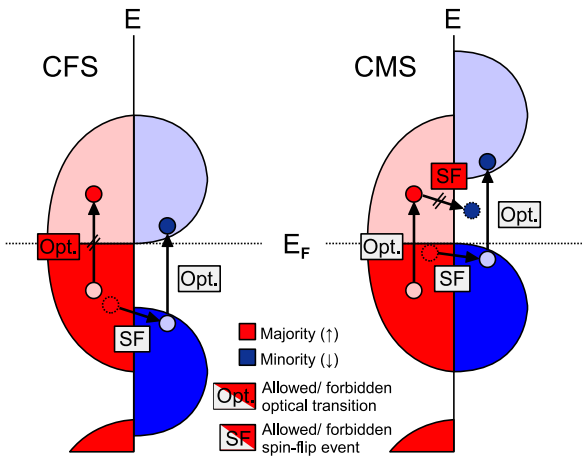

Figure 1. Schematic density of states of the Heusler compounds CFS and CMS. The band gap of CFS is mainly below E_F, for CMS it is mainly above [47]. Transitions induced by the optical pump pulse and spin-flip scattering pathways are schematically depicted according to [23]. Note that due to the specific band structure of CFS, no direct optical transitions are allowed in the majority channel with a photon energy of 1.5 eV (800 nm excitation). Reproduced with permission from [23]. Copyright (2010) by the American Physical Society.

annealing temperatures. Depending on the chemical ordering of the samples, we observe distinct changes in the magnetization dynamics. These only appear after the ultrafast demagnetization; that is, on a timescale of a few ten picoseconds. We explain these changes by spin-flip scattering of mostly thermalized majority electrons into unoccupied minority defect states. This additional spin-flip channel is mainly active in CMS, which explains the differences observed on the picosecond timescale between the demagnetization of CMS and CFS.

2. Methods

Changing the annealing temperature allows us to control the degree of chemical ordering in the studied compounds. The sample magnetic properties, together with their chemical ordering, have been carefully studied by a superconducting quantum interference device–vibrating sample magnetometer (SQUID–VSM), XRD, ellipsometry and MOKE. With TR-MOKE, we then measure the time evolution of the sample magnetization after optical excitation.

2.1. SQUID–VSM

Magnetometry measurements of the Heusler compound thin film samples were performed using a SQUID–VSM from quantum design with closed-cycle liquid He refrigeration (Evercool system). With this magnetometer, we measured the temperature dependent magnetization $M(T)$ for all samples in the range of 5–400 K for different applied field values in between 7 mT and 1 T. To check for the reproducibility of the results, we measured $M(T)$ during cool down and during the warm up and did not observe any significant differences. Furthermore, we first measured $M(T)$ in the temperature range 5–300 K for the as-deposited samples, to ensure that measurement temperatures of up to 400 K did not produce any sample modification. We did not detect any change in between both data series. The larger temperature range of up to 400 K is,

however, preferable for our data analysis because the extrapolation to T_C, which is substantially higher, is far more precise. We also measured magnetic hysteresis loops at different temperatures to properly estimate the diamagnetic background signal of the substrate and compensate our $M(T)$ data accordingly.

2.2. Static optical and magneto-optical characterization

We performed spectroscopic ellipsometry measurements of the studied Heusler compounds in the wavelength range of λ = 170–970 nm, using a GES5E VASE spectroscopic ellipsometer with automatic goniometer and *XYZ*-sample stage from Sopra. Specifically, we measured all of the samples at three different angles of incidence, namely 70°, 73° and 76° from normal incidence, to check for the consistency of the measurements and subsequent data analysis.

Furthermore, we monitored the magnetization reversal of the Heusler thin films with quasi-static MOKE. The MOKE magnetometer is equipped with a rotation stage, which allows the observation of the reversal curves as a function of the in plane angle between the crystal axes of the sample with respect to the applied magnetic field. The properties and the shape of the reversal curves allow us to make qualitative conclusions on the magnetic anisotropy present in the sample. Particularly, the coercive field as a function of the in-plane angle identifies the magnetic easy and hard axes, and also gives an indication on the magnitude of the crystalline anisotropy. The instrument is set up in the longitudinal MOKE configuration to access the in plane magnetization component. However, Heusler materials are known to show reasonably large quadratic MOKE (QMOKE), which makes it necessary to apply a symmetrization algorithm to extract the linear longitudinal MOKE signal from the measured signal. Additionally, the magnitude of the QMOKE present in the sample set was determined using a quadrupole magnet and perpendicular beam incidence. A detailed description of the working principle of the dual beam MOKE magnetometer, as well as the applied measurement procedures, can be found in [48].

2.3. TR-MOKE

The experiments on magnetization dynamics were carried out using a TR-MOKE pump-probe-setup. The laser system employed is a 800 nm, 1 kHz fs-amplifier system with a laser pulse duration of ≈60 fs at the sample position. More details on the setup can be found in [5, 11, 14]. The pump fluence for all measurements was approximately 15 mJ cm^{-2}. All of the data were recorded in the longitudinal Kerr geometry using a dichroic pump-probe setup. The samples have been saturated by using a magnetic field of approximately 10 mT. The Kerr rotation is detected using a balanced-bridge detector and a lock-in amplifier. An active beam stabilization and a double sample holder were used to ensure a consistent pump-probe overlap on the sample. In addition, the observed demagnetization at a few ps after time zero has been maximized each time after exchanging a sample to fine-tune the pump-probe overlap. The pump spot is over one order of magnitude larger than the probe spot, so that the material response is probed in a homogeneously excited area. All data are corrected for signal drift after the measurements. The signal drift correction is used to correct for a linear drift of the recorded signal. The algorithm is rather straightforward and relies on the way that data are recorded. Basically, one full recorded data loop consists of a list of n delay line steps from n_{min} to n_{max} and a single recording run moves the delay line from n_{min} to n_{max} and back to n_{min}. As n_{min} is in a time delay range before time zero (t = 0), the signal at n_{min} (t_{min}) and n_{min} (t_{max}), corresponding to M (t < 0), has to be

Table 1. Identifier labels, post-deposition annealing temperatures T_{ann}, magnetic moments μ_B and Curie temperatures T_C of the Heusler compound samples. Parameters of the short-time demagnetization as extracted from figures 4(c)–(d) are also given: τ_M is the demagnetization time constant; q is the magnetization quenching and b_s is the linear coefficient of the second demagnetization stage, present only in the CM_{300} and the CM_{amb} samples.

Identifier	T_{ann} (°C)	m_{exp} (μ_B/f.u.)	T_C (K)	τ_M(fs)	q (%)	b_s (ps)
CF_{500}	500	5.4 ± 0.1	975 ± 16	276 ± 8	54	—
CF_{300}	300	5.7 ± 0.1	1030 ± 28	250 ± 10	54	—
CF_{amb}	—	3.8 ± 0.1	908 ± 24	251 ± 5	55	—
CM_{500}	500	3.1 ± 0.1	970 ± 9	345 ± 4	63	—
CM_{300}	300	3.8 ± 0.1	808 ± 16	353 ± 7	61	78.1 ± 7.9
CM_{amb}	—	2.2 ± 0.1	610 ± 4	340 ± 3	65	34.7 ± 0.9

equal. The difference, if any, between the signals for $t < 0$ is then used to calculate a drift vector, which is used to correct the signal drift using the (real) time stamp recorded with each data point (which is important, as the time distance between two delay line steps depends on the step width). Data is only drift corrected in this way (and evaluated) if the total average signal on the photodiode does not change in any significant way during the measurement, as any loss of total signal points to either sample damage or a misalignment of the lasers system. Data not fulfilling this criterion is discarded.

3. Sample characterization

The CFS and CMS thin film samples studied here were grown in the following stacking structure [49]: Ta(3 nm)/Heusler(30 nm)/Ag(40 nm)/Cr(20 nm) on MgO (epitaxial ordering Heusler(001)[110]/Ag(001)[100]/Cr(001)[110]/MgO(001)[100]). All of the samples were deposited at room temperature in the same deposition run using magnetron-sputtering and subsequently annealed at 500 °C, 300 °C or left as-deposited (further called Cx_{500}, Cx_{300}, and Cx_{amb}, x either F or M for CFS and CMS, see table 1).

3.1. Structural characterization by XRD

The crystal structure of the samples was investigated using XRD. The XRD data for the CMS sample series is shown in figures 2(a)–(c). The three investigated samples show the B2 crystal structure. The degree of ordering increases with increasing annealing temperature. This is visible in the increase of the B2 (002) superstructure peak in the XRD spectrum in figure 2(a). The samples annealed at 500 °C additionally show the presence of the $L2_1$ phase (i.e., the highest ordering), as visible in the pole scan of the (111) lattice reflex in figure 2(b). Epitaxial growth is also verified by the pole scans of the (111), as well as (220) lattice reflexes (figure 2(c)), which are present for all cubic structure types. The results for CFS are shown in figures 2(d)–(f). They are are similar to the ones obtained for CMS. In particular, we only obtain $L2_1$ -ordering for the highest annealing temperature. Since the origin of the transformation from B2 to $L2_1$ structure in CFS (CMS) is an increase of the chemical ordering via suppression of Fe

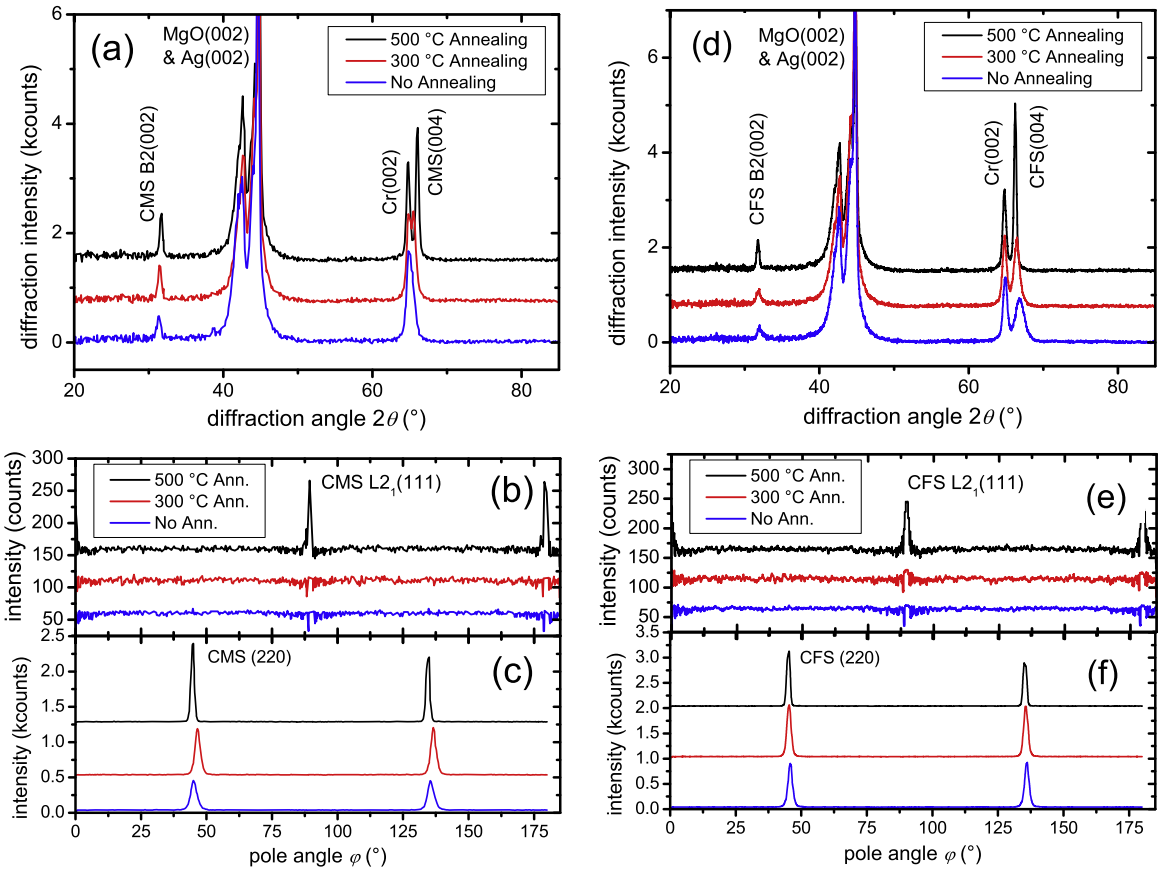

Figure 2. (a) $\theta - 2\theta$ XRD scan for the CMS annealing series samples, showing an increase in the B2-ordering with increasing annealing temperature. (b) Pole scan at the position of the CMS $L2_1$ superstructure peak, showing that $L2_1$-ordering is only present for the highest annealing temperature. (c) Pole scan of the CMS (220)-sample reflex showing epitaxial growth and the cubic sample structure. (d) $\theta - 2\theta$ XRD scan for the CFS annealing series samples, showing an increase in the B2-ordering with increasing annealing temperature. (e) Pole scan at the position of the CFS $L2_1$ superstructure peak, showing that $L2_1$-ordering is only present for the highest annealing temperature. (f) Pole scan of the CFS (220)-sample reflex showing epitaxial growth and the cubic sample structure. All of the data have been offset on the *y*-axis for clarity with decreasing annealing temperature from top to bottom.

(Mn)-Si intermixing [50], we can state that the defect density decreases with increasing the annealing temperature.

3.2. Magnetic characterization by SQUID–VSM

The magnetic properties of the samples were additionally investigated using SQUID–VSM measurements to determine both the magnetic moment in Bohr magnetons per formula unit [μ_B/f.u.] and the Curie temperature T_C. The Curie temperature was extrapolated from low-temperature *M(T)* measurements in the range 5–400 K by using the interpolation formula described in [51]. Please note that although the actual temperature regime of the respective Curie temperatures is not reached during these measurements (as it would irreversibly change

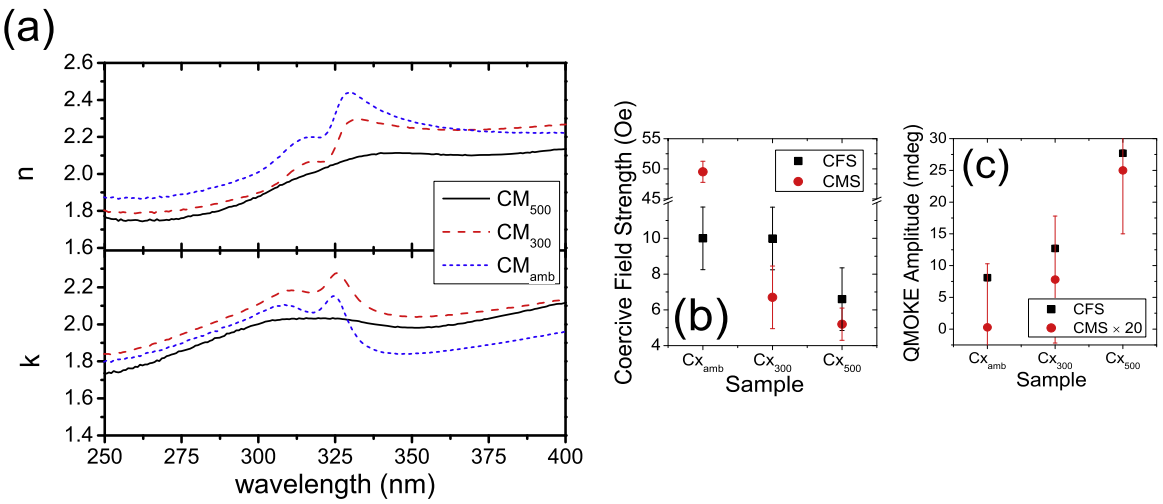

Figure 3. (a) Effective refractive index n and absorption coefficient k[6] from ellipsometry measurements of the CMS annealing series samples. In both refractive index and absorption coefficient data, a spectral feature at 325 nm is missing for the CM_{500} sample, which we associate with the plasma resonance of the Ag buffer layer, for further detail see the text. (b) Easy axis coercive fields of the CFS and CMS annealing series samples. Error bars are half of the magnetic field step width. (c) QMOKE amplitude $M_L M_T$ for CFS and CMS samples. The CMS signal is multiplied by a factor of 20 for visibility. Error bars correspond to the noise level at the detector.

the sample properties), the used evaluation routine allows to estimate T_C within an error of only a few percent. The values are given in table 1. For CFS, the annealed samples have magnetic moments deviating 10% or less from the theoretical Slater-Pauling value of 6.0 μ_B/f.u. and Curie temperatures comparable to those measured for high quality bulk samples, which is 1100 K [52, 53]. Like the XRD data, these results indicate an increased sample quality for the annealed samples.

For CMS the magnetic moments show a more intriguing behavior. The moment value for the highest annealing temperature (3.1 $\pm$ 0.1 μ_B/f.u.) shows a relatively strong deviation from the expected theoretical value of 5.0 μ_B/f.u. which we attribute to a partial alloying of the Ag buffer layer with CMS at the Ag/CMS interface. Evidence for such alloying processes at high annealing temperatures can be found in the literature [54]. In addition, our own ellipsometry measurements, shown in figure 3(a), reveal a strong smearing out of the Ag plasma resonance at 3.8 eV photon energy for the CM_{500} -sample in comparison to the other two samples. (The full set of results from the ellipsometry measurements can be found in the appendix). This strongly indicates alloying according to [55]. The alloying at the interface leads to a lower magnetic film thickness than expected or even partial antiferromagnetic coupling in the Ag/Heusler interface region of the film, as known for Mn [56]. Such effects lead, in turn, to a systematically underestimated magnetic moment from the SQUID–VSM measurements[5]. At the same time T_C increases throughout the whole series and reaches about the bulk value of 985 K measured for a high-quality CMS single crystal [57] for the CM_{500} -sample. Considering the depth-dependent

[5] To estimate the volume-averaged saturation magnetization, the total magnetic volume has to be known. If part of the assumed magnetic volume is non-magnetic, then the obtained volume-averaged saturation magnetization will be lower than the real one.

generation of the MOKE signal, discussed in detail in [58], most of the signal in our static and TR-MOKE measurements should originate from the upper 15 nm of the Heusler compound layer at our chosen probe wavelength of 400 nm. Therefore, it is unlikely that the possibly alloyed interface region will contribute substantially to the measured MOKE signals. In addition, this interface might not even be ferromagnetic anymore.

3.3. Magnetic characterization by quasi-static MOKE

The magnetization reversal curves of the films using quasi-static MOKE show that the coercivity of all films decreases with increasing annealing temperature (see figure 3(b)), reaching very low values of less than 7 Oe in the easy axis direction for the films with the highest annealing temperatures. Such a trend with annealing temperature was connected to a decrease of the magneto-crystalline anisotropy and an increase in $L2_1$ -order for another Heusler film system [59]. In the present systems, similar considerations of a decreasing anisotropy constant in correlation with the increased ordering of the films can be applied. We further observe that the QMOKE signal of the films strongly increases with annealing temperature (see figure 3(c)), which is also linked to the appearance of the $L2_1$ phase. In fact, according to [59, 60], with higher disorder the optical transitions responsible for the QMOKE are broadened and no effect can be observed, while for higher crystal order the well defined symmetry and spin–orbit coupling can lead to a large QMOKE signal.

3.4. Static characterization summary

Our sample characterization data show that the chemical ordering of all our samples increases with increasing annealing temperature. In particular, increasing the annealing temperature progressively reduces Fe (Mn)-Si intermixing in CFS (CMS), leading to a higher degree of $L2_1$ order. The only deviation from this behavior was found for the measured magnetic moment of CM_{500}, which we explained by a partial alloying of Ag and CMS at the Ag/CMS-interface, leading to a systematically underestimated magnetic moment. We thus conclude that, for all of the samples, the defect densities decrease with increasing annealing temperature. We can now study the influence of the chemical ordering on ultrafast magnetization dynamics.

4. Dynamical characterization

Figures 4(a)–(b) show the results of the TR-MOKE measurements for the CFS and CMS annealing series. In order to capture the complete magnetization dynamics (ultrafast demagnetization and recovery back to equilibrium), we have recorded the transient MOKE

[6] For simplicity, we have transformed our experimental spectroscopic ellipsometry results into an effective optical constant (n,k) based upon the assumption of a single bulk-like optically isotropic material. Given the thickness of the individual layers, this simple analysis does not provide extremely accurate optical constants for the Heusler compounds (even though all three measurements using different angles of incidence give consistent n and k values with about 1% precision for all samples), but it does allow for the observation of the plasma resonance coming from the Ag template layer and its modification due to high temperature annealing and it is, therefore, an excellent probe for the onset of interface diffusion in the CMS/Ag interface, as can be clearly seen in figure 3(a).

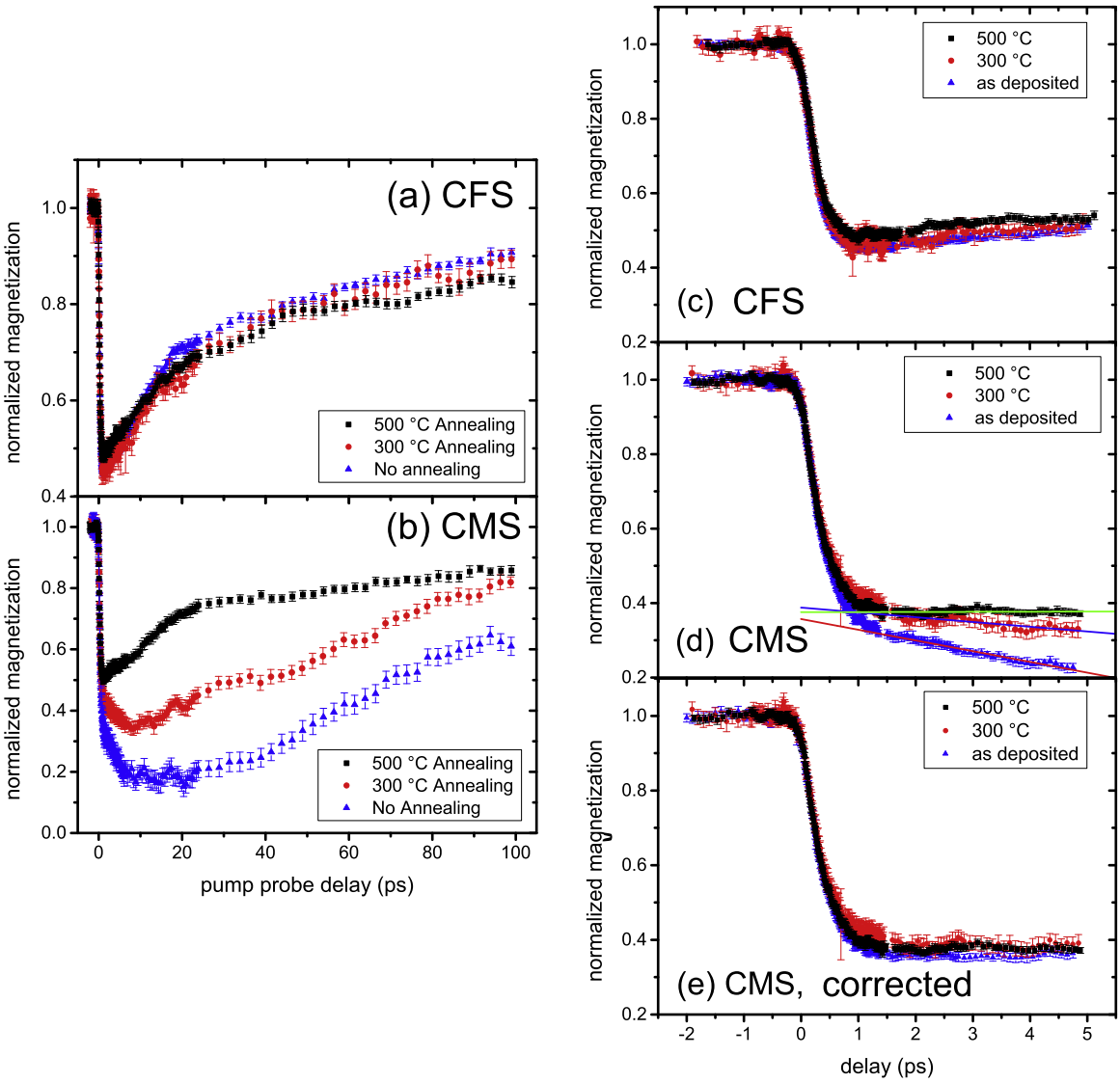

Figure 4. Long-term demagnetization dynamics for: (a) the CFS and (b) the CMS annealing series. Short-term magnetization dynamics of the CFS (c) and of the CMS (d) thin film samples. The lines are linear fits to the second decay, for details see text; (e) data from (d) with subtracted second stage. Measurements were performed with identical excitation fluences in all cases. Error bars are statistical errors.

signal for delay times up to 100 ps. A quick inspection of figures 4(a)–(b) reveals a strong influence of the annealing temperature for the dynamics measured for the CMS annealing series, but not for the CFS annealing series. The three CFS curves (figure 4(a)) show a virtually identical behavior (within the experimental error), characterized by a simple exponential decay followed by a magnetization recovery that takes place in two stages: a fast component up to approximately 25 ps followed by a slow component.

In the CMS data (figure 4(b)), magnetization recovery still consists of two stages, with the faster stage visible up to 25 ps. The shape of the recovery is, however, strongly influenced by the annealing temperature. The three CMS samples also show differences on shorter

timescales. In order to discuss this behavior, we have measured the demagnetization dynamics with a better signal-to-noise ratio for delays up to 5 ps. The results are shown in figures 4(c)–(d).

The CFS annealing series (figure 4(c)) also shows virtually identical dynamics on a short-term time scale. In contrast, the CMS annealing series (figure 4(d)) shows a similar initial demagnetization on a timescale of a few hundred femtoseconds for all three samples, followed by differences in the dynamics on the picosecond timescale. More specifically, the CM_{300} (red circles) and the CM_{amb} (blue triangles) sample show a second, slower demagnetization stage. This stage is more pronounced for the as-deposited sample. The CM_{500} sample (black squares) does not exhibit this second stage. Its magnetization stays at a constant level for at least 5 ps after the initial demagnetization and is fairly similar in shape to data published in [23].

To better compare the initial demagnetization stage, we subtracted the second demagnetization stage by using the slope of the linear fits depicted in figure 4(d)[7]. The result is depicted in figure 4(e). The demagnetization curves for all three graphs now look virtually identical, indicating that the two demagnetization stages occurring up to 5 ps after optical excitation occur nearly independently.

The short term demagnetization was then analyzed by least squares fitting an exponential decay of the general form $q \times \exp\left(-t/\tau_M\right)$, which was additionally convolved with a gaussian to account for the finite laser pulse duration. Here, q is the strength of demagnetization (or magnetization quenching) and τ_M is the time constant of demagnetization. The extracted parameters are given in table 1. Similar demagnetization time constants are reported for CMS samples annealed at 300, 400 and 450 °C by Liu *et al* but for much smaller quenchings of a few percent [24]. However, the authors did not quantitatively evaluate or discuss this behavior.

We can extract a further parameter for the CMS annealing series: the time constants of the linear fit of the second demagnetization stage b_s. In particular, the coefficient b_s was determined as the slope of the linear fit of the decay of the magnetization after the initial ultrafast dynamics decay has stopped; that is, starting at 1600 fs. We find 34.7 ± 0.9 ps for the as-deposited sample and about 78.1 ± 7.9 ps for the CM_{300} sample, see also table 1. For the well annealed sample, the linear coefficient is zero within the error bars. (Please note that compared to the short-range measurement reported in figure 4, the the long-term measurement for the CM_{500} sample in figure 4 shows a slight recovery in the first 5 ps, with a linear coefficient of 1.05×10^{-5}. This slight difference between the long-range and short-range measurement is due to the fact that the long-range measurement has been performed for a slightly weaker laser excitation, as is evident from the smaller magnetization quenching in this curve.)

5. Discussion

We now interpret the results displayed in figure 4. First of all, the initial demagnetization step for all studied samples is similar, regardless of the degree of chemical ordering. Therefore, we

[7] The linear fit to the data is performed in the time delay range starting at about 1600 fs because the influence of the initial delay step is then negligible. The signal correction has the form: corrected_signal = original_signal − slope_{LinFit} × Delay. The subtraction is applied in the range from time zero to 5 ps.

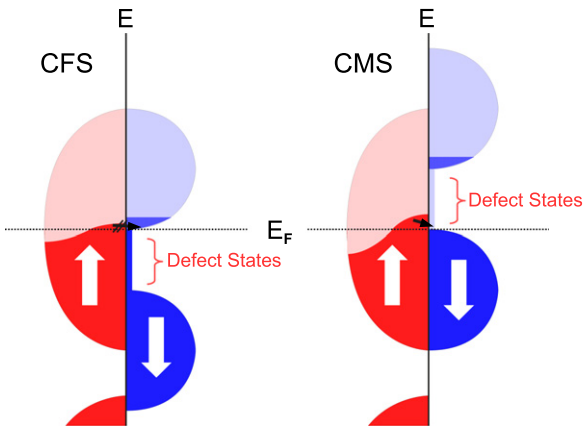

Figure 5. Schematic density of states of the Heusler compounds (a) CFS and (b) CMS considering an additional density of states induced by defects, and population of the states after optical excitation and thermalization of electrons. The unoccupied DOS is light shaded, occupied DOS dark shaded. Black arrows designate either allowed or forbidden (crossed out) spin-flip electron dynamics.

conclude that the ordering does not have much influence on the main demagnetization channel. This is surprising since it was assumed that structural disorder leading to defect states enhances the phase-space for spin-flip scattering and speeds up magnetization dynamics [22].

We can, however, understand this behavior considering the explanation given in [23]. Figure 1 reproduces the main result of this publication. Ultrafast demagnetization in the studied Heusler compounds happens because of optical excitation in the minority DOS. Subsequently, majority electrons scatter into the empty minority states below E_F and lead to ultrafast demagnetization. Spin-flip dynamics of excited majority electrons above the Fermi level are of minor importance because they are forbidden because of the minority band gap in CMS and do not take place in CFS, since the excitation energy of 1.55 eV is too low for optical excitation in the majority channel. Therefore, to interpret the data shown here we have to consider two main points: first, optical excitation occurs mostly (CMS) or exclusively (CFS) in the minority channel [47]; and secondly, spin-flip dynamics of majority electrons in empty minority states below E_F is the reason for ultrafast demagnetization. Within this picture, an additional low density of states of defects sites, leading to a smearing out of the gap (see figure 5), will not considerably influence the ultrashort demagnetization dynamics. The highly effective hole-mediated spin-flip dynamics below E_F is thus the dominating channel on short timescales, even in the samples with lower chemical ordering (high defect concentrations).

Having understood the ultrafast dynamics, we will now analyze the behavior of CFS and CMS on the time scale up to 5 ps (figures 4(c)–(d)). As we are now basically discussing picosecond dynamics, we first have to understand which electronic states will contribute to the magnetization dynamics on this time-scale. In particular, we want to address here the origin of the second demagnetization stage observed in the CMS samples with low chemical ordering; that is, large number of defects. First of all, we recall that in [23] it has been shown that the minority bands just above the band gap depopulate very slowly, on the picosecond time scale.

This means that during the second demagnetization stage, the minority bands above the band gap will still be significantly populated, as schematically depicted in figure 5. This means that in CFS the spin-flip of mostly thermalized majority electrons into unoccupied minority bands is not efficient because the minority bands are still transiently substantially populated. This scattering process is completely suppressed in CMS since just above E_F there are no minority states due to the presence of the band gap.

Let us now consider the influence of defect states located in the band gap of CFS and CMS, which are mainly due to the B2 disorder present in the non-annealed, as well as in the samples annealed at low temperature (see section 3.1). Defect states in the minority band gap of CFS will be mostly populated in the considered time scale. They will thus not contribute to the magnetization dynamics in the picosecond range, which is in agreement with our experimental observations. In CMS, on the other hand, spin-flip scattering of mostly thermalized majority electrons into unoccupied minority defect states will be a still active demagnetization channel (see figure 5), this can explain the observed second slope in the demagnetization curves. The stronger second stage in the as-deposited sample compared to the sample annealed at 300 °C (see figure 4(d)) originates from the lower chemical ordering, that is, a higher amount of defect sites (equivalent to a larger scattering phase space) allowing for a higher number of spin-flips of majority electrons in a given time interval. Furthermore, the additional free phase space from these defects explains why the total demagnetization of both CM_{300} and CM_{amb} is higher than in CM_{500}. In CFS, these defects are occupied prior to optical excitation; thus, they do not represent additional phase space for scattering because the number of minority hole states is only given by the constant number of absorbed photons. In conclusion, we can ascribe the second demagnetization stage to spin-flip processes taking place from mostly thermalized majority electrons into empty minority defect states within the half-metallic gap above E_F, as schematically depicted in figure 5. Since the second stage is absent in the CM_{500} -sample, this may be seen as an indirect proof of half-metallicity in structurally well-ordered CMS [63].

Lastly, we discuss a recently proposed second mechanism for ultrafast demagnetization, superdiffusive transport [7, 9, 17–19], and its influence on the dynamics observed in the Heusler samples used here. Superdiffusive transport basically explains ultrafast demagnetization through the different lifetimes or mean free paths and high velocities of highly excited majority and minority carriers, which leads to a net transport of the longer-living majority electrons [61, 62] away from the probed sample region [7, 9]. This mechanism is not believed to be of importance here for two reasons. First of all, there are no highly excited electrons in the majority DOS of CFS and CMS for our photon energy of 1.55 eV, due to the peculiarities of the band structure [23, 47]. This means that both the high velocity of carriers and the secondary electrons from electron–electron scattering, which contribute to this process, are absent. Secondly, due to the presence of a band gap in the minority channel, the minority electrons that are laser-excited to just above the gap will have longer lifetimes than any excited majority carriers [64]. Therefore, we would actually expect an increase in magnetization from minority carriers leaving the probed sample area. On the other hand, the low group velocity of the carriers in these bands could prevent the occurrence of such an effect. Overall, we thus conclude that spin transport is not of relevance in the samples studied here.

6. Conclusion

We studied the influence of defects on the magnetization dynamics of the carefully characterized Heusler compounds CFS and CMS by comparing the samples with different degrees of chemical ordering. We find no influence of defect states on the ultrafast demagnetization, which shows that hole-mediated spin-flip scattering is the dominant mechanism on this timescale. Furthermore, we explained the different magnetization dynamics of CFS and CMS on the picosecond timescale by the different energetic position of the minority band gap. In CMS, structural disorder leads to unoccupied density of states within the gap. In-scattering of excited majority electrons into these additional states leads to the second demagnetization stage that was observed experimentally for CMS samples with low chemical ordering. We argue that the absence of this stage in the well-ordered CMS sample may be seen as an indirect proof of the half-metallicity of this sample.

Acknowledgments

We wish to thank Hans Christian Schneider and Steffen Kaltenborn for helpful discussion on the subject of lifetimes of excited electrons in half metallic Heusler compounds. We gratefully acknowledge the DFG for funding within the Research Training Group GRK 792 and Research Units FG559 and the Strategic Japanese-German Joint Research Program ASPIMATT. Work at nanoGUNE was supported through funding from the Basque Government under program no. PI2012-47 and the Spanish MICINN under project no. MAT2012-36844. OI acknowledges funding from the Basque Government fellowship no. BFI09.284.

Appendix. Full ellipsometry data

Spectroscopic ellipsometry measurements of the studied Heusler compounds were performed in the wavelength range of λ = 170–970 nm, using a GES5E VASE spectroscopic ellipsometer with automatic goniometer and *XYZ*-sample stage from Sopra. All of the samples were measured at three different angles of incidence, namely 70°, 73° and 76° from normal incidence, to check for the consistency of the measurements and subsequent data analysis. For simplicity, the experimental spectroscopic ellipsometry results were then transformed into an effective optical constant (n,k), assuming a single bulk-like optically isotropic material. Given the thickness of the individual layers, this simple analysis does not provide extremely accurate optical constants for the Heusler compounds (even though all three measurements using different angles of incidence give consistent n and k values with about 1% precision for all samples), but it does allow for the observation of spectral features such as the plasma resonance coming from the Ag template layer and its modification due to high temperature annealing in the CM_{500} -sample (right part of figure A1) and it is, therefore, an excellent probe for the onset of interface diffusion at the CMS/Ag interface, whereas no such effect is found for the CFS annealing series samples (left part of figure A1).

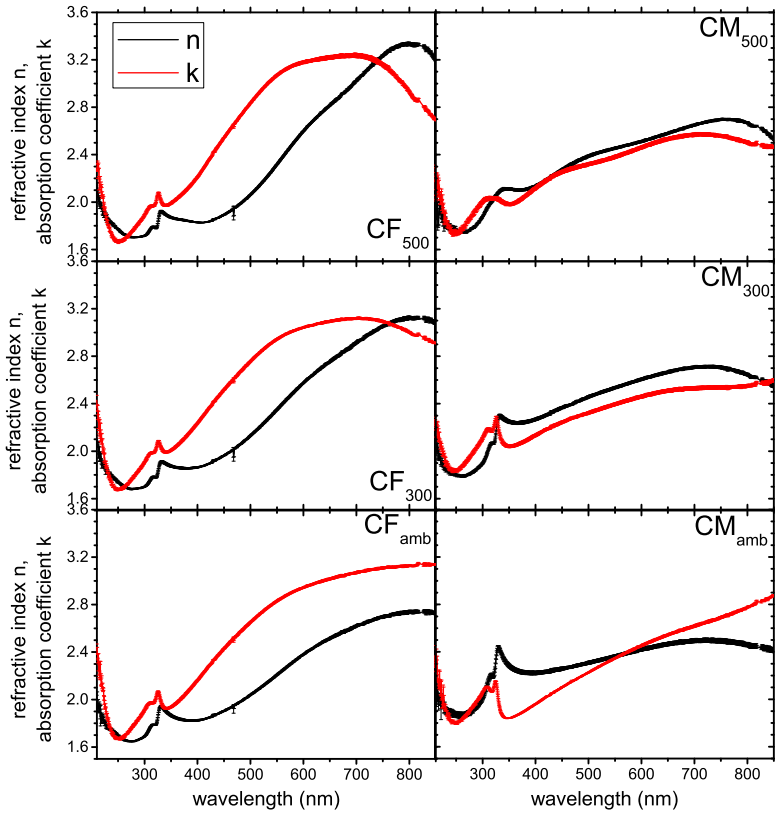

Figure A1. Effective refractive index n and absorption coefficient k from ellipsometry measurements of the CFS and CMS annealing series samples. For details on the measurement evaluation, see text.

References

[1] Beaurepaire E, Merle J-C, Daunois A and Bigot J-Y 1996 Ultrafast spin dynamics in ferromagnetic nickel *Phys. Rev. Lett.* **76** 4250–3

[2] Koopmans B, Kicken H H J E, van Kampen M and de Jonge W J M 2005 Microscopic model for femtosecond magnetization dynamics *J. Magn. Magn. Mater.* **286** 271–5

[3] Zhang G P and Hübner W 2000 Laser-induced ultrafast demagnetization in ferromagnetic metals *Phys. Rev. Lett.* **85** 3025–8

[4] Steiauf D and Fähnle M 2009 Elliott-Yafet mechanism and the discussion of femtosecond magnetization dynamics *Phys. Rev.* B **79** 140401

[5] Krauß M, Roth T, Alebrand S, Steil D, Cinchetti M, Aeschlimann M and Schneider H C 2009 Ultrafast demagnetization of ferromagnetic transition metals: the role of the coulomb interaction *Phys. Rev.* B **80** 180407(R)

[6] Bigot J-Y, Vomir M and Beaurepaire E 2009 Coherent ultrafast magnetism induced by femtosecond laser pulses *Nat. Phys.* **5** 515–20

[7] Battiato M, Carva K and Oppeneer P M 2010 Superdiffusive spin transport as a mechanism of ultrafast demagnetization *Phys. Rev. Lett.* **105** 027203

[8] Essert S and Schneider H C 2011 Electron-phonon scattering dynamics in ferromagnetic metals and their influence on ultrafast demagnetization processes *Phys. Rev.* B **84** 224405

[9] Battiato M, Carva K and Oppeneer P M 2012 Theory of laser-induced ultrafast superdiffusive spin transport in layered heterostructures *Phys. Rev.* B **86** 024404

[10] Rhie H-S, Dürr H A and Eberhardt W 2003 Femtosecond electron and spin dynamics in *ni/w* (110) films *Phys. Rev. Lett.* **90** 247201
[11] Cinchetti M, Albaneda M S, Hoffmann D, Roth T, Wüstenberg J-P, Krauß M, Andreyev O, Schneider H C, Bauer M and Aeschlimann M 2006 Spin-flip processes and ultrafast magnetization dynamics in co: unifying the microscopic and macroscopic view of femtosecond magnetism *Phys. Rev. Lett.* **97** 177201
[12] Stamm C *et al* 2007 Femtosecond modification of electron localization and transfer of angular momentum in nickel *Nat. Mater.* **6** 740–3
[13] Carpene E, Mancini E, Dallera C, Brenna M, Puppin E and de Silvestri S 2008 Dynamics of electron-magnon interaction and ultrafast demagnetization in thin iron films *Phys. Rev.* B **78** 174422
[14] Koopmans B, Malinowski G, Dalla Longa F, Steiauf D, Fahnle M, Roth T, Cinchetti M and Aeschlimann M 2009 Explaining the paradoxical diversity of ultrafast laser-induced demagnetization *Nat. Mater.* **9** 259
[15] Roth T, Schellekens A J, Alebrand S, Schmitt O, Steil D, Koopmans B, Cinchetti M and Aeschlimann M 2012 Temperature dependence of laser-induced demagnetization in Ni: a key for identifying the underlying mechanism *Phys. Rev.* X **2** 021006
[16] Mathias S *et al* 2012 Probing the timescale of the exchange interaction in a ferromagnetic alloy *Proc. Natl. Acad. Sci. USA* **109** 4792–7
[17] Rudolf D *et al* 2012 Ultrafast magnetization enhancement in metallic multilayers driven by superdiffusive spin current *Nat. Commun.* **3** 1037
[18] Eschenlohr A, Battiato M, Maldonado P, Pontius N, Kachel T, Holldack K, Mitzner R, Fhlisch A, Oppeneer P M and Stamm C 2013 Ultrafast spin transport as key to femtosecond demagnetization *Nat. Mater.* **12** 332–6
[19] Turgut E *et al* 2013 Controlling the competition between optically induced ultrafast spin-flip scattering and spin transport in magnetic multilayers *Phys. Rev. Lett.* **110** 197201
[20] Wietstruk M, Melnikov A, Stamm C, Kachel T, Pontius N, Sultan M, Gahl C, Weinelt M, Dürr H A and Bovensiepen U 2011 Hot-electron-driven enhancement of spin-lattice coupling in gd and tb 4*f* ferromagnets observed by femtosecond x-ray magnetic circular dichroism *Phys. Rev. Lett.* **106** 127401
[21] Fähnle M and Illg C 2011 Electron theory of fast and ultrafast dissipative magnetization dynamics *J. Phys.: Condens. Matter* **23** 493201
[22] Müller G M *et al* 2009 Spin polarization in half-metals probed by femtosecond spin excitation *Nat. Mater.* **8** 56–61
[23] Steil D, Alebrand S, Roth T, Krauß M, Kubota T, Oogane M, Ando Y, Schneider H C, Aeschlimann M and Cinchetti M 2010 Band-structure-dependent demagnetization in the Heusler alloy $Co_2Mn_{1-x}Fe_xSi$ *Phys. Rev. Lett.* **105** 217202
[24] Liu Y, Shelford L R, Kruglyak V V, Hicken R J, Sakuraba Y, Oogane M and Ando Y 2010 Optically induced magnetization dynamics and variation of damping parameter in epitaxial Co_2MnSi Heusler alloy films *Phys. Rev.* B **81** 094402
[25] Wüstenberg J-P, Steil D, Alebrand S, Roth T, Aeschlimann M and Cinchetti M 2011 Ultrafast magnetization dynamics in the half-metallic Heusler alloy $Co_2Cr_{0.6}Fe_{0.4}Al$ *Phys. Status Solidi* B **248** 2330–7
[26] Mann A *et al* 2012 Insights into ultrafast demagnetization in pseudogap half-metals *Phys. Rev.* X **2** 041008
[27] Meng K K, Wang S L, Xu P F, Chen L, Yan W S and Zhao J H 2010 Magnetic properties of full-Heusler alloy Co2Fe1xmnxal films grown by molecular-beam epitaxy *Appl. Phys. Lett.* **97** 232506
[28] Cheng C, Meng K, Li S, Zhao J and Lai T 2013 Femtosecond laser excitation of multiple spin waves and composition dependence of gilbert damping in full-Heusler $Co_2Fe_{1-x}Mn_xAl$ films *Appl. Phys. Lett.* **103** 232406
[29] Stanciu C D, Kimel A V, Hansteen F, Tsukamoto A, Itoh A, Kirilyuk A and Rasing Th 2006 Ultrafast spin dynamics across compensation points in ferrimagnetic GdFeCo: the role of angular momentum compensation *Phys. Rev.* B **73** 220402
[30] Stanciu C D, Hansteen F, Kimel A V, Kirilyuk A, Tsukamoto A, Itoh A and Rasing Th 2007 All-optical magnetic recording with circularly polarized light *Phys. Rev. Lett.* **99** 047601

[31] Vahaplar K, Kalashnikova A M, Kimel A V, Hinzke D, Nowak U, Chantrell R, Tsukamoto A, Itoh A, Kirilyuk A and Rasing Th 2009 Ultrafast path for optical magnetization reversal via a strongly nonequilibrium state *Phys. Rev. Lett.* **103** 117201

[32] Radu I *et al* 2011 Transient ferromagnetic-like state mediating ultrafast reversal of antiferromagnetically coupled spins *Nature* **472** 205–8

[33] Steil D, Alebrand S, Hassdenteufel A, Cinchetti M and Aeschlimann M 2011 All-optical magnetization recording by tailoring optical excitation parameters *Phys. Rev.* B **84** 224408

[34] Ostler T A *et al* 2012 Ultrafast heating as a sufficient stimulus for magnetization reversal in a ferrimagnet *Nat. Commun.* **3** 666

[35] Alebrand S, Bierbrauer U, Hehn M, Gottwald M, Schmitt O, Steil D, Fullerton E, Mangin S, Cinchetti M and Aeschlimann M 2014 Subpicosecond magnetization dynamics in TbCo alloys *Phys. Rev.* B **89** 144404

[36] Žutić I, Fabian J and Sarma S D 2004 Spintronics: fundamentals and applications *Rev. Mod. Phys.* **76** 323–410

[37] Bader S D and Parkin S S P 2010 Spintronics *Annu. Rev. Condens. Matter Phys.* **1** 71–88

[38] Mangin S *et al* 2014 Engineered materials for all-optical helicity-dependent magnetic switching *Nat. Mater.* **13** 286–92

[39] Graf T, Felser C and Parkin S S P 2011 Simple rules for the understanding of Heusler compounds *Prog. Solid State Chem.* **39** 1–50

[40] Mizukami S, Tsunegi S, Kubota T, Oogane M, Watanabe D, Naganuma H, Ando Y and Miyazaki T 2010 Ultrafast demagnetization for Ni 80 Fe 20 and half-metallic Co_2MnSi Heusler alloy films *J. Phys. Conf. Ser.* **200** 042017

[41] Picozzi S, Continenza A and Freeman A J 2004 Role of structural defects on the half-metallic character of *Co_2MnGe* and *Co_2MnSi* Heusler alloys *Phys. Rev.* B **69** 094423

[42] Picozzi S and Freeman A J 2007 Polarization reduction in half-metallic Heusler alloys: the effect of point defects and interfaces with semiconductors *J. Phys.: Condens. Matter* **19** 315215

[43] Bruski P, Erwin S C, Ramsteiner M, Brandt O, Friedland K-J, Farshchi R, Herfort J and Riechert H 2011 Disorder-induced reversal of spin polarization in the Heusler alloy Co_2FeSi *Phys. Rev.* B **83** 140409

[44] Ozdogan K and Galanakis I 2011 Effect of order on the half-metallic gap in Heusler compounds *J. Appl. Phys.* **110** 076101

[45] Rodan S *et al* 2013 Nuclear magnetic resonance reveals structural evolution upon annealing in epitaxial Co_2MnSi Heusler films *Appl. Phys. Lett.* **102** 242404

[46] Ouardi S *et al* 2009 Electronic properties of Co_2MnSi thin films studied by hard x-ray photoelectron spectroscopy *J. Phys.* D: Appl. Phys. **42** 084011

[47] Balke B, Fecher G H, Kandpal H C, Felser C, Kobayashi K, Ikenaga E, Kim J-J and Ueda S 2006 Properties of the quaternary half-metal-type Heusler alloy $Co_2Mn_{1-x}Fe_xSi$ *Phys. Rev.* B **74** 104405

[48] Trudel S, Wolf G, Schultheiß H, Hamrle J, Hillebrands B, Kubota T and Ando Y 2010 Note: probing quadratic magneto-optical Kerr effects with a dual-beam system *Rev. Sci. Instrum.* **81** 026105

[49] Sato J, Oogane M, Naganuma H and Ando Y 2011 Large magnetoresistance effect in epitaxial $Co_2Fe_{0.4}Mn_{0.6}Si$/Ag/$Co_2Fe_{0.4}Mn_{0.6}Si$ devices *Appl. Phys. Express* **4** 113005

[50] Graf T, Felser C and Parkin S S P 2011 Simple rules for the understanding of Heusler compounds *Prog. Solid State Chem.* **39** 1–50

[51] Kuz'min M D, Chernyshov A S, Pecharsky V K, Gschneidner K A and Tishin A M 2006 Temperature dependence of the ferromagnetic order parameter in Gd, Tb, and Dy *Phys. Rev.* B **73** 132403

[52] Wurmehl S, Fecher G H, Kandpal H C, Ksenofontov V, Felser C, Lin H-J and Morais J 2005 Geometric, electronic, and magnetic structure of Co_2FeSi: Curie temperature and magnetic moment measurements and calculations *Phys. Rev.* B **72** 184434

[53] Wurmehl S, Fecher G H, Kandpal H C, Ksenofontov V, Felser C and Lin H-J 2006 Investigation of Co_2FeSi: the Heusler compound with highest curie temperature and magnetic moment *Appl. Phys. Lett.* **88** 032503

[54] Sakuraba Y, Izumi K, Bosu S, Saito K and Takanashi K 2011 Temperature dependence of spin-dependent transport properties of Co_2MnSi-based current-perpendicular-to-plane magnetoresistive devices *J. Phys. D: Appl. Phys.* **44** 064009

[55] Nilsson P O, Lindau I and Hagström S B M 1970 Optical plasma-resonance absorption in thin films of silver and some silver alloys *Phys. Rev.* B **1** 498–505

[56] Kallmayer M, Elmers H J, Balke B, Wurmehl S, Emmerling F, Fecher G H and Felser C 2006 Magnetic properties of Co_2Mn1-xFexSi Heusler alloys *J. Phys. D: Appl. Phys.* **39** 786–92

[57] Brown P J, Neumann K U, Webster P J and Ziebeck K R A 2000 The magnetization distributions in some Heusler alloys proposed as half-metallic ferromagnets *J. Phys.: Condens. Matter* **12** 1827

[58] Traeger G, Wenzel L and Hubert A 1992 Computer experiments on the information depth and the figure of merit in magnetooptics *Phys. Status Solidi* A **131** 201–27

[59] Trudel S, Wolf G, Hamrle J, Hillebrands B, Klaer P, Kallmayer M, Elmers H-J, Sukegawa H, Wang W and Inomata K 2011 Effect of annealing on $Co_2FeAl_{0.5}Si_{0.5}$ thin films: a magneto-optical and x-ray absorption study *Phys. Rev.* B **83** 104412

[60] Wolf G, Hamrle J, Trudel S, Kubota T, Ando Y and Hillebrands B 2011 Quadratic magneto-optical Kerr effect in Co_2MnSi *J. Appl. Phys.* **110** 043904

[61] Aeschlimann M, Bauer M, Pawlik S, Weber W, Burgermeister R, Oberli D and Siegmann H C 1997 Ultrafast spin-dependent electron dynamics in fcc co *Phys. Rev. Lett.* **79** 5158–61

[62] Knorren R, Bennemann K H, Burgermeister R and Aeschlimann M 2000 Dynamics of excited electrons in copper and ferromagnetic transition metals: theory and experiment *Phys. Rev.* B **61** 9427–40

[63] Jourdan M *et al* 2014 Direct observation of half-metallicity in the Heusler compound Co_2MnSi *Nat. Commun.* **5** 3974

[64] Kaltenborn S and Schneider H C 2014 Spin-dependent lifetimes and nondegenerate spin-orbit driven hybridization points in Heusler compounds *Phys. Rev.* B **89** 115127